



Transparent Electrodes for Energy Storage Devices

Libin Wang^[a] and Xianluo Hu^{*[a]}

Transparent energy-storage devices have aroused interest because of the ever-increasing demands of transparent electronics. Transparent energy-storage electrodes (TESEs) are indispensable for emerging cutting-edge products and have thus attracted remarkable attention in the past decade. This minireview begins by introducing the basic evaluation metrics for TESEs. Then, recent progress of various types of TESEs such as carbonaceous materials, polymers, MXenes, and other

conductive substrates-based TESEs is outlined. In order to provide some inspiration and guidelines, we focus on summarizing the presently proposed strategies towards high-performance TESEs together with the applications of transparent supercapacitors. At the end of this minireview, we discuss the outlook and perspectives towards the development of transparent energy-storage devices.

1. Introduction

Modern aesthetic appeal and emerging transparent electronics necessitate the rapid development of high-end products with excellent optical transparency.^[1] Transparent conductive electrodes (TCEs) with both excellent light transmittance and electrical conductivity have been widely used in information and energy technologies including liquid crystal displays, touch panels, interactive electronics, photovoltaics, and window glass.^[2–5] Ever since the first attempt to investigate transparent conductive oxides in 1907, tin-doped indium oxide (ITO) has so far become the most successful and dominated material for TCEs.^[2] Within the past century, different materials have been applied to construct TCEs with high optoelectronic properties such as carbon nanotubes (CNTs), graphene, conducting polymers, and metallic grids.^[6–9] Despite the long history and great success in TCEs, the development of transparent energy-storage electrodes (TESEs) is hysteretic and sluggish.^[10,11]

Unlike the conventional monofunctional TCEs, both good electrical and capacitive figure-of-merits (termed as FoM_e and FoM_c , respectively) are required for TESEs. The former FoM_e evaluates their optoelectronic properties. At fixed transparency, a higher FoM_e indicates a lower equivalent series resistance (R_{ESR}) and therefore a better power output of TESEs. The latter FoM_c , however, reveals the energy-storage capabilities of transparent electrodes. Unfortunately, there exists a tradeoff between high transparency and good electrochemical performance in TESEs due to the percolation issue.^[12] In other words, the high transparency of TESEs is usually achieved at the expense of energy and power, as both the R_{ESR} and volumetric capacitance (C_v) become thickness-dependent when thickness falls below a threshold. Such a tradeoff presents great challenges for constructing desirable TESEs.

[a] L. Wang, Prof. X. Hu
State Key Laboratory of Materials Processing and Die & Mould Technology
School of Materials Science and Engineering
Huazhong University of Science and Technology
Wuhan 430074, China
E-mail: huxl@mail.hust.edu.cn

To the purpose of realizing high-performance TESEs, various materials have been exploited up to now, which can be classified as either conductive substrates-free or –based TESEs, as shown in Figure 1a. Materials of choice for conductive substrates-free TESEs including CNTs, graphene, conducting polymers, and MXenes, are both electroactive and electrically conductive so that they can serve as current collectors without

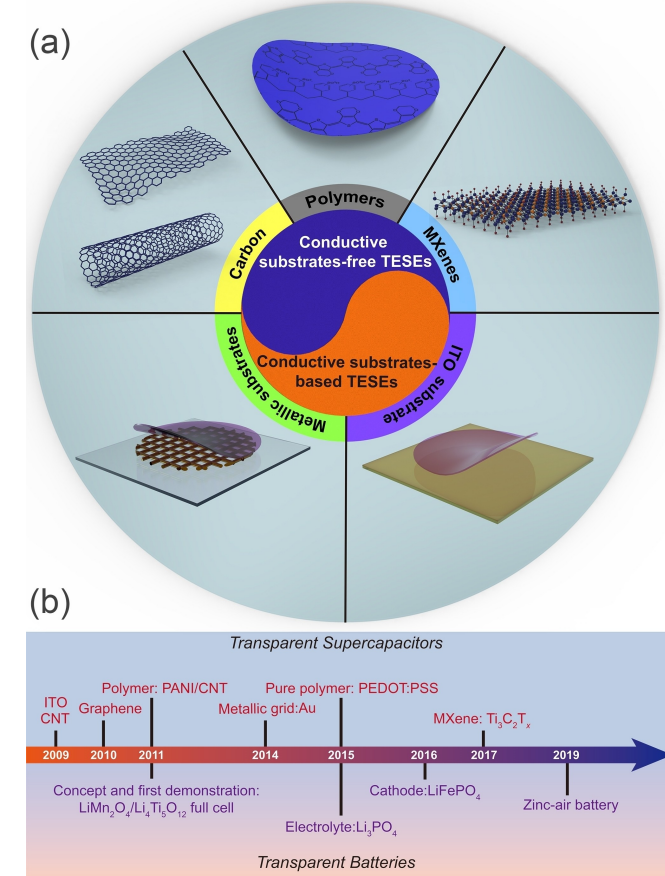


Figure 1. a) Summary of various types of TESEs. b) Timeline of the development of transparent supercapacitors and batteries.

extra conductive networks. Alternatively, conducting layer of ITO or metallic grids cooperating with capacitive materials is another class of TESEs. Of noticeable thing is that such a considerable progression is achieved within the near decades as outlined in Figure 1b, showing intense interests of research in this field. Taking transparent supercapacitors as an example, after the first demonstration of CNT/In₂O₃ as a TESE in 2009,^[13] various materials of choice involving ITO,^[14] graphene,^[15] metallic grid,^[16] PEDOT:PSS,^[17] and MXenes,^[18] successively emerged as significant candidates. On the contrary, the development of transparent batteries is restrained in its infancy stage due to the following reasons: 1) Transparent batteries require all the components including electrode materials, electrolytes, current collectors, separators as well as packing to be transparent, none of which are transparent except the electrolyte. 2) Most of cathode and anode materials are good absorbers even when the thickness is reduced below 1 μm, bringing difficulties in making them transparent by reducing the film thickness. 3) To powder portable electronics, batteries have a critical requirement in the thickness of electrode material (appr. 100 μm-1 mm), which is much larger than their optical absorption length. As a result, only limited attempts have been tried in transparent batteries.^[19-22] In this regard, our emphasis focuses on transparent supercapacitors.

The present minireview has systematically summarized the development of TESEs. We initiate the discussion by introducing the basic evaluation metrics for TESEs. After that, the present TESEs based on different materials of choice are reviewed and compared to highlight their advantages and disadvantages. Besides, general routes to improve the figure-of-merits as well as functional properties of TESEs are summarized. Last but not least, we discuss challenges and perspectives towards the future development of TESEs.

2. Evaluation Metrics of TESEs

There are several parameters that optically and electrochemically affect the performance of TESEs as mentioned above. Ideally, TESEs should possess high transparency (T), low sheet resistance (R_s), and high capacitance. Nevertheless, the percolation effect that both the sheet resistance and capacitance are thickness-dependent in the high-transparency region presents a common challenge for constructing high-performance TESEs.^[12,23] The widely adopted way to achieve high transparency by decreasing the thickness of active materials will



Libin Wang received his B.S. degree in functional materials at Huazhong University of Science and Technology (HUST) in 2015 and is currently a Ph.D. candidate under the supervision of Prof. Xianluo Hu. His research focuses on the fabrication of nanomaterials and the design of miniaturized functional supercapacitors.

result in a higher R_s and lower capacitance, showing the trade-off between them. Besides, when it comes to a commercial scale, mechanical and chemical stability, cost, and other functional properties (flexibility and stretchability) should also be taken into consideration.

2.1. Electrical Figure-of-Merit (FoM_e)

To facilitate the comparison of electrical properties, a well-accepted variation is proposed by Coleman et al., termed as electrical figure-of-merit (FoM_e) that is determined by the ratio of DC to optical conductivity (σ_{dc}/σ_{op}).^[23] Though initially proposed for the study of TCEs, the FoM_e is also applicable for TESEs. The FoM_e can be obtained through the following Eq. (1):

$$T = \left(1 + \frac{188.5 \sigma_{op}}{R_s \sigma_{dc}}\right)^{-2} \quad (1)$$

One can calculate the FoM_e by fitting a series of T vs. R_s data. Note that T is defined as the transmittance of electrodes at the wavelength of 550 nm. A higher FoM_e indicates better electrical conductivity at high transparency and therefore a lower R_{ESR} , corresponding to a better power performance of TESEs.

2.2. Capacitive Figure-of-Merit (FoM_c)

More importantly, as power sources, the charge-storage capacity of TESEs is of significance. As mentioned above, an excellent energy-storage capability must compromise transparency. To evaluate the energy-storage properties, a capacitive figure-of-merit (FoM_c), calculated by the ratio of volumetric capacitance to optical conductivity (C_V/σ_{op}), is proposed. The correlation between FoM_c and T can be expressed as follows [Eq. (2)]:

$$T = \left[1 + \frac{188.5}{C_V} \sigma_{op} C_A\right]^{-2} \quad (2)$$

in which, C_A is the intrinsic areal capacitance of the electrode. By measuring a series of T and C_A , the FoM_c (F S cm⁻²) can be obtained. The higher the FoM_c is, the better the charge storage property is in TESEs at given transparency. Convenient to the comparison of FoM_c among reported works, all the FoM_c in this



Xianluo Hu is a full professor of Materials Science and Engineering at Huazhong University of Science and Technology (HUST). He received his Ph.D. from Chinese University of Hong Kong (CUHK) in 2007 and worked as a Postdoctoral Researcher in CUHK and National Institute of Materials Science (NIMS) of Japan from 2007 to 2009. His current research interests focus on electrochemical energy-storage materials and devices.

minireview is roughly calculated using an individual C_A and T . Besides, the C_A of electrodes and energy density of symmetric transparent supercapacitors are obtained according to Equations (3) and (4), respectively:

$$C_{A, \text{electrode}} = 4 \times C_{A, \text{device}} \quad (3)$$

$$E = C_{A, \text{device}} \times \Delta V^2 / (2 \times 3600) \quad (4)$$

where $C_{A, \text{device}}$, $C_{A, \text{electrode}}$, E , and ΔV are the areal capacitance of the device, areal capacitance of the electrode, energy density, and operating window of supercapacitors, respectively.

2.3. Stability

The sustainable working of energy-storage devices under different stress and surrounding conditions is a key evaluation for their practical applications. Therefore, both mechanical and electrochemical stability may be the limitations of TESEs. To start with, under deformations, the fall of active materials and the loss of electrical contact within electrodes will lead to severe capacity degradation and even failure. Secondly, during a long-term working period, the conductive layer, metallic grid, for example, will confront chemical corrosion when exposed to moisture.^[24,25] Finally, as for some pseudocapacitive materials, the structural collapse and dissolution of active materials into electrolytes during the charge/discharge process result in an apparent deterioration of electrochemical performance.^[26,27] All these issues should be considered and deserve efforts to warrant a considerable potential of TESEs for practical applications.

2.4. Cost

To date, the most successful material for TCEs is ITO owing to its low R_s ($10\text{--}100 \Omega/\text{sq}$) at transparency higher than 85%. However, the high production cost originating from the scarcity of indium and high-temperature treatment during production becomes the main drawback of ITO-based TCEs and TESEs. Apart from ITO, TESEs based on other materials are investigated in lab-scale and adequate attention has not yet been attached to their cost. Generally speaking, most reported TESEs suffer from their high cost owing to the expensive materials (e.g., Au grids and MXenes) and complicated preparation, especially in an industrial scale-up. Recently, Wu's group proposed a roll-to-roll method for mass production of Ag network TCEs via blow spinning without post-treatment.^[28] Such a green and economical method is promising for the fabrication of next-generation TCEs.

2.5. Other Functional Properties

The trend of developing portable and wearable electronics promotes the continued growth of supercapacitors with out-

standing flexibility and stretchability. Thus, TESEs with functional properties such as flexibility and stretchability are highly demanded in modern society. The intrinsic brittleness of ITO hinders its application where mechanical flexibility is required. To this end, various types of flexible and stretchable TESEs based on nanostructured materials,^[29] elastomer substrate,^[30] and nanostructured electrodes^[27,31] have been developed successfully (details will be discussed in Section 4). Currently, the achieved highest stretchability in transparent supercapacitors is around 160% stretching,^[25] which demands more efforts in this field.

3. Different Types of TESEs

Electrode materials for TESEs should possess both good electrical conductivity and high charge-storage capability at high transparency. Electroactive materials with intrinsic high conductivity are the preferred materials of choice such as CNTs, graphene, conducting polymers, and MXenes. When used as TESEs, no extra conductive substrates are needed, thus being classified as conductive substrates-free TESEs. On the contrary, because of their poor electrical conductivity, most pseudocapacitive materials must be integrated into a conductive layer (metallic grids or ITO), which are defined as conductive substrates-based TESEs. However, current TESEs suffer from the trade-off between high transparency and high electrochemical performance in TESEs on account of the limitation of the percolation effect. In this section, to provide a comprehensive understanding of the development of TESEs, we first discuss the percolation effect. Then, different types of TESEs as well as their applications in transparent supercapacitors will be introduced.

3.1. Percolation Effect

Regarding the materials for TESEs, they are intrinsically non-transparent. A general method to make them transparent is reducing the thickness of films. When the thickness is reduced to its percolation limits, however, the percolation effect occurs as shown in Figure 2a. Generally, as shown in Figure 2b, the relationship between T and R_s in the bulk-like region can be described as Eq. (1).^[32] However, when it comes to the high-transparency region, the so-called percolation region, with the increase of T , the R_s increases dramatically, which no longer satisfies such a relationship. This issue is defined as the percolation effect. When transparent electrodes encounter the percolation problem, it indicates that high FoM_e can only be achieved at transparency with a low level. In the high-transparency region, however, FoM_e decreases rapidly, which is disadvantageous to get high-performance TESEs with high transparency. Besides, the percolation threshold can be estimated. Taking graphene as examples, the electrical percolation indicates a severely worse electrical performance when the thickness is reduced below a critical value. The percolation threshold (N_c) is displayed in Eq. (5):

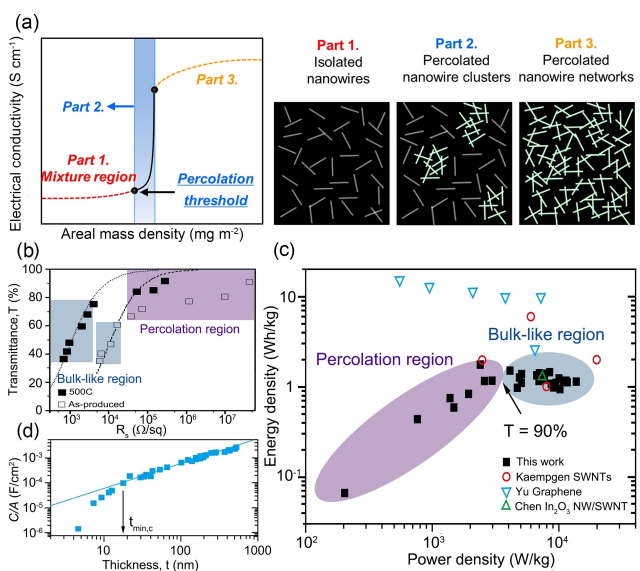


Figure 2. a) Schematic illustration of percolation effect. Reproduced with permission from Ref. [4]. Copyright (2020) Zhengzhou University. b) Transmittance (@550 nm) plotted as a function of R_s for both as-produced and annealed (500 °C) films. The dashed lines are fits to Eq. (1) and are defined by $\sigma_{dc}/\sigma_{op}=0.04$ and $\sigma_{dc}/\sigma_{op}=0.4$ for as-produced and annealed film, respectively. Reproduced with permission from Ref. [32]. Copyright (2010) Wiley-VCH. c) Areal capacitance plotted as a function of thickness. d) Ragone plot comparing the data described in this paper to other transparent supercapacitors described in the literature. (c,d) Reproduced with permission from Ref. [12]. Copyright (2012) American Chemical Society.

$$N_c = 4.236^2 \pi L_s^2 \approx 1/L \quad (5)$$

where L_s and L are the individual length and the aspect ratio of the graphene, respectively. A smaller N_c suggests a low surface coverage to form a path and conduct the charge carriers, which means high conductivity can be obtained at high transmittance. To get a smaller N_c , materials with high electrical conductivity and high aspect ratio are needed.

Apart from the electrical percolation, there exists a capacitive percolation for TESEs. As Coleman et al. found in CNT films, the area capacitance should be linearly changed with the thickness in the absence of electron and ion transport limitation, which is valid for those in the bulk-like region.^[12] Below a critical thickness ($t_{min,c}$), there is an apparent deviation and the percolation effect becomes dominant (Figure 2c). The percolation effect presents a limitation to the electrical and capacitive properties of TESEs. In Figure 2d, it is clear that supercapacitors based on the thickness in the bulk-like region exhibit a better energy/power density than that of the ones in the percolation region. It is thus concluded that to maximize the power and energy density for high transparent electrodes, percolation issue should be avoided to extend the bulk-like region, and the $t_{min,c}$ must be reduced as much as possible. For electrical percolation, it is known that N_c is controlled by the distribution of junction resistances within the networks. Regarding the capacitive percolation, however, it is still unclear what parameters dominate the threshold.

3.2. Conductive Substrate-Free TESEs

Given that the transparency, FoM_c , and energy density are the critical evaluations for TESEs and related transparent devices, we make a summary to compare these factors of different types of TESEs. The results are shown in Figure 3.

In virtue of the high conductivity, high aspect ratio (~1000), good mechanical flexibility, CNTs have been considered to be a promising candidate for TESEs. The great success in TCEs with high FoM_e up to 82.7 facilitates CNTs to be the first demonstration in transparent supercapacitors prior to the use of all kinds of other materials.^[13] After that, tremendous efforts have been made to improve both FoM_e and FoM_c of CNTs-based TESEs.^[12,30,33–35] Many parameters can be optimized to obtain an enlarged FoM_e such as wall number, diameter, bundle length of CNTs, or even fabrication methods.^[36] According to Eq. 5, N_c represents the surface coverage to form a path and conduct the charge carriers. The charge carriers within CNTs film, indeed, flow along a tube and then pass to adjacent tubes via the junctions, which means that the sheet resistance consists of contact resistance on the junctions and the intrinsic resistance of tubes. Therefore, to achieve high FoM_e and avoid the percolation problem, CNTs with small wall numbers, large aspect ratio, and well-defined orientation are desired.^[37,38] Unfortunately, the FoM_c (~2 F cm⁻²) of reported CNTs-based TESEs is rather low due to the limited electrical double-layer capacitors-type (EDLC) capacitance.^[39] Through hybridizing CNTs with pseudocapacitive materials can boost the capacitance, the achieved FoM_c and energy density are still way too low.^[40,41]

Monolayered graphene exhibits high transparency of 97.7% that is appealing for transparent electronics. Nevertheless, similar to CNTs, graphene suffers from their low intrinsic capacitance when used as TESEs.^[15,29,42–45] Pure graphene-based TESEs usually possess a low areal capacitance (10–500 μF cm⁻²) and FoM_c (< 1.5 F cm⁻²).^[46–48] Reported works suggest that the FoM_c can be enlarged either by structural engineering or hybridizing with high-capacitance pseudocapacitive materials.^[49–53] For example, Wang's group has proposed a NaCl-templated method to fabricate graphene with different morphologies. The as-prepared graphene displays a 3D porous structure with a large surface area and showcases a high FoM_c ranging from ~12.4 to 20.7 when applied in TESEs.^[49–51] Recently, Zhang and co-workers demonstrated that hybridizing graphene with metal oxides is an effective way to achieve high FoM_c . Through solution assembly, graphene-wrapped Ni(OH)₂ nanosheets show a high areal capacitance of 49.25 mF cm⁻² at high transparency of 72.3% (@550 nm), corresponding to a high FoM_c of 52.7 F cm⁻².^[52] When assembled into a symmetric solid-state supercapacitor, a high energy density of 2.6 μWh cm⁻² at the transparency of 51% is obtained. However, as revealed by Coleman's group, graphene-based TESEs would encounter percolation problems.^[32] This means, as for the construction of TESEs with both high FoM_c and high transparency, graphene is struggling. Besides, as shown in Figure 3a and b, carbonaceous materials usually have high transparency, but the FoM_c and energy density of devices are rather low.

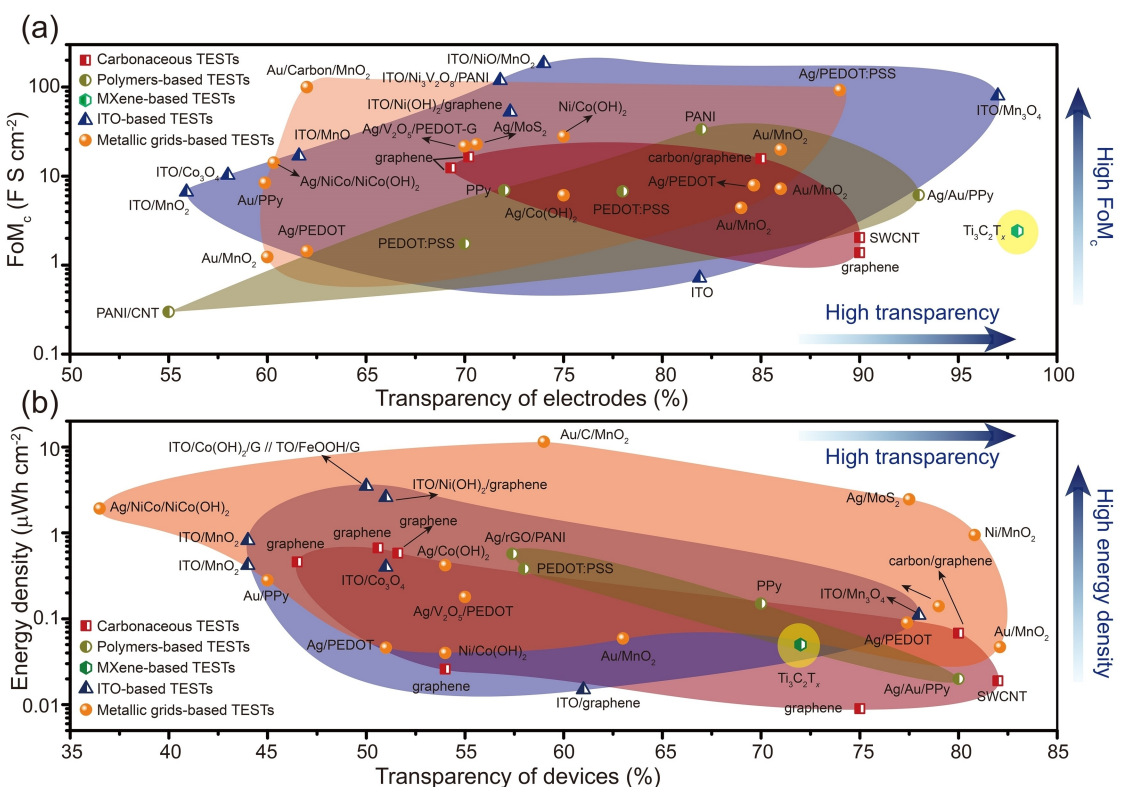


Figure 3. a) FoM_c plotted as a function of transparency for reported TESEs. b) Energy density plotted as a function of transparency for reported transparent devices. Note that unless specified, the transparent devices are symmetrically assembled based on the mentioned TESEs.

In addition to carbonaceous materials, conductive polymers have also been explored in TESEs thanks to their low optical conductivity, high electrical conductivity, and good energy-storage capability.^[54–61] For example, by integrating into a Ni mesh, PEDOT:PSS-based TESE realizes an extremely high FoM_c of 10000 at high transparency of 84%.^[62] More importantly, Coleman and his teammates found that no percolation issue is confronted for PEDOT:PSS films even at high transparency of 99%, showing the great promise of PEDOT:PSS-based TESEs. Of noticeable shortcoming is the low FoM_c for most of the reported polymers-based TESEs due to the low areal capacitance. The areal capacitances are restrained below 10 mF cm^{-2} and FoM_c is below 7 FScm^{-2} .^[17,55,57,59,61] Encouragingly, a hybrid PANI-rGO–Ag electrode reported by Sun's group displays a high areal capacitance of 25.6 mF cm^{-2} (calculated from the symmetric device) and a FoM_c of $\sim 38 \text{ FScm}^{-2}$ at a transmittance of 78.7%, opening an avenue for boosting the capacitive performance of polymers-based TESEs.^[54]

As mentioned before, to avoid the electrical and capacitive percolation problems, materials with high conductivity and capacitance are highlighted. Recently, MXenes become a rising star and attract remarkable attention in this field.^[18,63–67] MXenes represent a class of transition metal carbides and/or carbonitrides that are obtained by selectively removing the A layer within their parent layered MAX phases, where the M is an early transition metal (e.g., Sc, Ti, Zr, Hf, V, Nb, Ta, Cr, Mo), A represents a group 13 or 14 (e.g., Al, Si, Ga, Ge, In) element, and X is C and/or N. The theoretical metallic conductivity of

MXenes can reach to $8 \times 10^5 \text{ S m}^{-1}$. More importantly, the percolation issue can be avoided for MXenes-based TESEs as found in Zhang's work.^[18] When used as TESEs, the $\text{Ti}_3\text{C}_2\text{T}_x$ film with high transparency of 98% exhibits an areal capacitance of 0.13 mF cm^{-2} , rendering a calculated FoM_c of 2.4 FScm^{-2} . Nevertheless, only limited MXenes have been investigated as TESEs so far.^[18,65]

3.3. Conductive Substrate-Based TESEs

Conductive substrates like ITO and metallic grids usually display impressively high FoM_e (e.g., 120–240 for ITO and 500 for Ag grid) and have aroused intensive interests.^[2,23] The charge-storage capability of these conductive substrates is negligible so that they need to cooperate with other electroactive materials to gain a high FoM_c .^[26,68–73] Owing to the high FoM_e , the FoM_c of ITO-based TESEs stands on a pole position among various types of TESEs (Figure 3a). For example, Yim et al. fixed well-defined Mn_3O_4 nanoparticles onto an ITO substrate in the presence of 1,2-ethanedithiol.^[74] The as-prepared Mn_3O_4 /ITO electrode with 3 deposition cycles shows a high capacitance of 6.5 mF cm^{-2} with high transparency of 97%. Thus, the FoM_c is calculated to be 79.8 FScm^{-2} , much higher than most conductive substrates-free TESEs. The FoM_c of ITO-based TESEs can be further elevated by forming binary heterostructures with high capacitance. More recently, Yang's group has integrated binary hybrids of $\text{Ni}_3\text{V}_2\text{O}_8@\text{PANI}$ and $\text{NiO}@\text{MnO}_2$ onto ITO

substrates.^[75,76] The fabricated ITO@Ni₃V₂O₈@PANI and ITO@NiO@MnO₂ electrodes show high FoM_c of 119 and 184 FScm⁻², respectively. Despite these high capacitive properties, the very nature of brittleness of ITO hampers their application in flexible electronics.

Considering the high aspect ratio of nanowires, metallic grids are believed to be more desirable for portable and flexible electronics. To date, various metallic grids have been developed and applied in TESEs, including Ag,^[24,27,77-87] Au,^[16,88-91] Ni,^[92-94] and so on. Many of them exhibit good mechanical stability, flexibility, and even stretchability.^[25,31,95-97] Generally, as shown in Figure 3a, the FoM_c of metallic grids-based TESEs is high, ranging from 0.5 to 167 FScm⁻². Moreover, the energy density of devices based on metallic grids-based TESEs can be high due to the high areal capacitance of the electrode. The highest energy density in Figure 3b is achieved based on Au/C/MnO₂ electrodes, delivering a high value of 11.5 μ Whcm⁻² at the transmittance of 59%.^[98] However, as unveiled in previous works, metallic grids, for example, the Ag grid, would encounter the percolation issue. Thus, though high FoM_c can be obtained, the transparency of metallic grids-based TESEs is somehow low (usually below 85%). Besides, the chemical stability of metallic networks is also challenging for practical applications.

4. Strategies Towards High-Performance TESEs

High-performance TESEs with high optical transparency, high FoM_c, and excellent stability together with flexibility and stretchability are urgently needed for transparent electronics and thus of significance. In this section, we point out the key points of enhancing the performance of TESEs and summarize the recently proposed strategies towards high-performance TESEs, as shown in Figure 4.

According to Eq. (2), one can gain a high FoM_c by either increasing the transparency or areal capacitance of TESEs. For improving the optical transmittance, strategies like material

engineering and patterning design are proposed. For example, tuning the orientation of carbonaceous materials through material engineering is a feasible means for boosting the transparency of TESEs.^[37,38] Jiang et al. revealed that CNTs with super-aligned morphology possess ultrahigh transparency of 83% with a sheet resistance of 1 k Ω sq⁻¹, which is much superior to conventional CNTs films.^[37] Similarly, Wang's group proposed a NaCl-templated method to tailor the nanostructure of the graphene film (Figure 5a). As shown in Figure 5b and 5c, the fabricated micro-structured interconnected ribbon-like graphene foam (MRG-GF) shows a 3D ordered porous structure, achieving a high FoM_c (20.7 FScm⁻²) at 72% transmittance for the electrode.^[49] As for conductive substrates-based TESEs, enhancing the transmittance of conductive networks is advantageous to achieve high FoM_c.^[16,62,94] Through patterning design, the area for photon transmitting can be enlarged while maintaining its conductivity. Thus, random distributed metallic patterns inspired by leaves or cracks have been designed.^[89,90] Representative, Kulkarni et al. reported a template method to fabricate a highly transparent Au electrode by using a crackle-templated separator (Figure 5d).^[89] The randomly distributed Au network provides adequate surface area for light transmission, thus showcasing a high transmittance of 81% after the electrodeposition of MnO₂. Besides, a symmetric transparent supercapacitor assembled by sandwiching two Au/MnO₂ electrodes exhibits high transparency of 64% (Figure 5e). Interestingly, the transparency of the supercapacitor can be further improved via engineering the cell configuration, as revealed in the same work. By fabricating Au/MnO₂ on both sides of the separator (Figure 5f), a symmetric supercapacitor can be directly constructed with electrodes on either side, displaying a high optical transmittance of 78% that is much higher than that of conventionally sandwiched devices (Figure 5g). Very recently, Wang and his co-workers have done impressive work on the patterning design of the Ni mesh. As shown in Figure 6a-c, the Ni substrates fabricated by laser direct-writing patterning exhibit highly conductivity (3×10^4 S cm⁻¹), high transparency (>84% transmittance), and very high FoM_c.

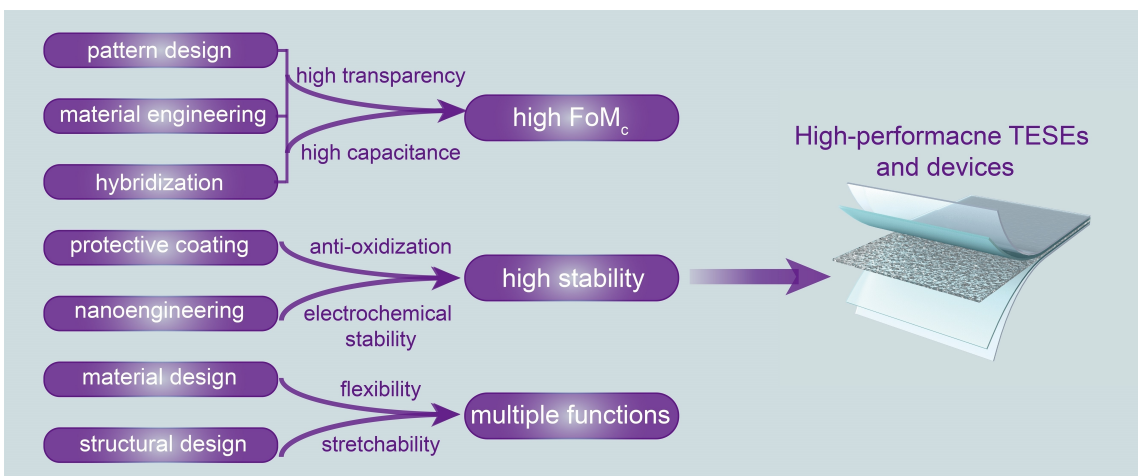


Figure 4. Strategies towards high-performance TESEs and devices.

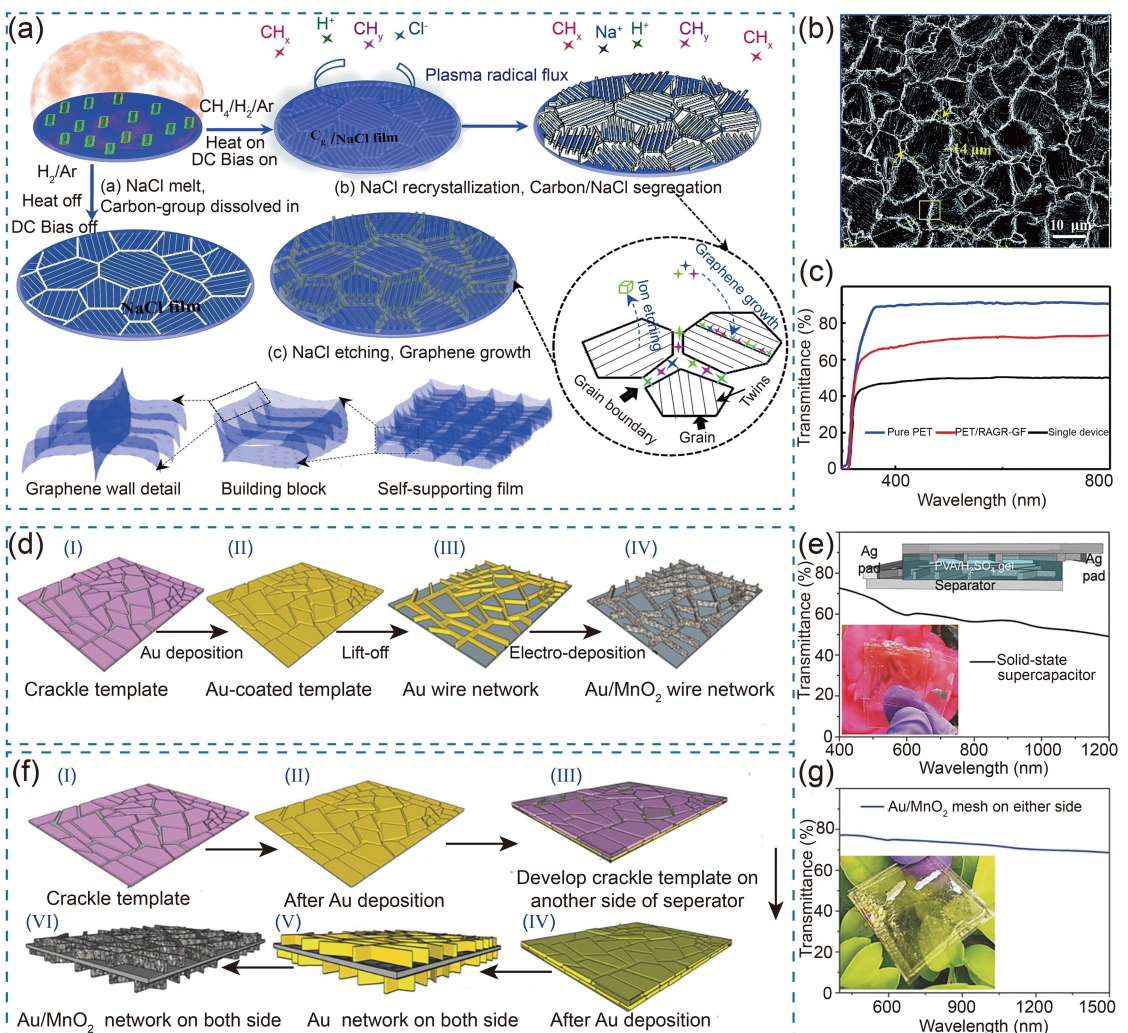


Figure 5. a) Schematic illustration of the preparation and sample model of the regularly aligned graphene ribbon-based transparent and flexible film. The first step, (1) the NaCl powder bathed in the plasma ball was thoroughly melted with carbon groups dissolved in the melts. Second, (2) NaCl recrystallized with the temperature drop, while carbon-groups segregated from NaCl grains and gathered at the grain boundary. (3) Graphene ribbons nucleated and grew along the grain boundaries accompanied by the NaCl etching process. b) SEM image of the fabricated MRG-GF. c) Transmittance spectra of the MRG-GF and device. (a-c) Reproduced with permission from Ref. [49]. Copyright (2017) Royal Society of Chemistry. d) Schematic illustration for the fabrication of the Au/MnO₂ wire network on the separator. e) Transmittance spectra of the sandwiched symmetric device. Inset is the digital photograph of the device. f) Schematic illustration of various steps to fabricate Au/MnO₂ on both sides of the separator. g) Transmittance spectra of the supercapacitor with electrodes on both sides. Inset is the digital photograph of the device. (d-g) Reproduced with permission from Ref. [89]. Copyright (2017) Wiley-VCH.

(167 F cm⁻²).^[94] In addition to transmittance, areal capacitance is also crucial for FoM_c. As mentioned before, the areal capacitance of graphene is rather low, so that the FoM_c is usually below 1.5 F cm⁻². However, molecular engineering via introducing *p*-aminophenol into interlayers as active species is capable of triggering a 20-fold enhancement in areal capacitance.^[46] Besides, hybridizing with high-capacity materials is a commonly used means to boost the areal capacitance. To this end, many pseudocapacitive materials such as RuO₂,^[53] MnO₂,^[71] Mn₃O₄,^[74] V₂O₅,^[87] Ni(OH)₂,^[95] Co(OH)₂,^[93] and so on, have been applied as active materials for TESEs, realizing high FoM_c even over 100 F cm⁻².

The chemical and electrochemical stability is essential for the practical application of TESEs. When used in the atmosphere, the aging of active materials and current collectors would result in a severe deterioration of electrodes. For

instance, MXenes can be easily oxidized in an open-air, which significantly limited their application conditions. Besides, conductive layers like ITO and metallic networks are also unstable when exposed. Ag grid is one of the most commonly used conductive layers owing to their high conductivity and facile preparation. To improve the anti-oxidation of Ag networks, introducing some chemically inert layers as protective coatings such as graphene,^[79] Au,^[24,27] and Ni,^[82] has been demonstrated to be a valid strategy. Ko et al. fabricated core-shell structured Ag–Au nanowires, consisting of Ag core and a very thin layer of Au. In virtue of the inert nature of Au, the Ag–Au network prepared through filtration exhibits excellent stability with negligible resistance increase when placed in a moist environment for four weeks.^[24] Aside from the chemical stability, attention should also be paid to the electrochemical stability of pseudocapacitive materials. A typical example is V₂O₅, which

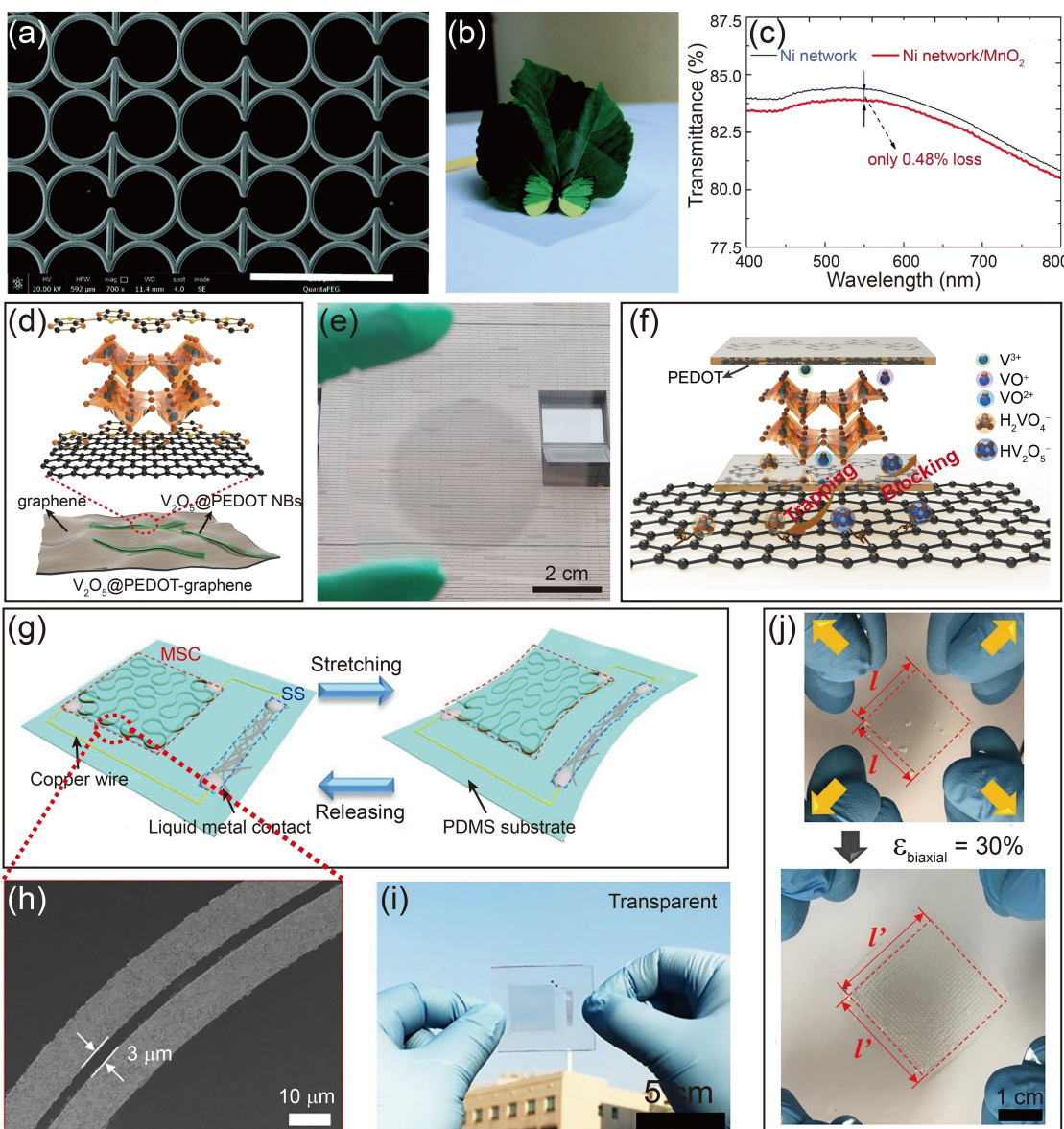


Figure 6. a) SEM image of the freestanding Ni network electrode. Scale bar: 400 nm. b) Digital photographs of the freestanding Ni network electrode. c) Transmittance spectra of the freestanding Ni network electrode before and after MnO₂ electrochemical deposition. (a–b) Reproduced with permission from Ref. [94]. Copyright (2017) Royal Society of Chemistry. d) Schematic illustration of V₂O₅@PEDOT-graphene. e) Digital photograph of the V₂O₅@PEDOT-graphene on polyethylene terephthalate. f) Proposed mechanism for the exceptional durability of transparent electrodes. (d–f) Reproduced with permission from Ref. [87]. Copyright (2020) Elsevier. g) Schematic illustration of a transparent and stretchable microsupercapacitor (MSC) integrated with an Ag NW strain sensor (SS). h) Magnified SEM image of fractal-designed electrodes. i) Digital photograph of the fabricated fractal-designed stretchable device. j) Digital photograph of the stretching process. (g–j) Reproduced with permission from Ref. [31]. Copyright (2020) Elsevier.

suffers from severe dissolution and structural collapse during the charge/discharge process. Very recently, our group has developed an ultrastable transparent electrode based on V₂O₅@PEDOT-graphene hybrids (Figure 6d).^[87] Nanoengineering via the strong coupling between PEDOT and graphene enables the assembly of the well-defined structure of hybrids as well as the formation of transparent film (Figure 6e). It is found that both the kinetic blocking of the PEDOT layer and the anchoring capability of graphene upon soluble vanadium ions contribute synergistically to the electrochemical stability, rendering a long lifespan over 150,000 cycles (Figure 6f).

To meet the demands of flexible and wearable electronics, tremendous effort has been devoted to enhancing the flexibility and stretchability of TESEs. Current approaches for developing stretchable TESEs can be either categorized as “materials that stretch” or “structures that stretch”.^[25,29–31,45,49] Conductive materials with a high aspect ratio usually display good stretchability and flexibility when integrated with elastomeric matrices. These materials include CNTs,^[30] conducting polymers,^[90] and metallic nanowires.^[25] However, the material of choice that is intrinsically stretchable is still limited. In contrast, structural design toward stretchable TESEs has little requirements on the material of choice. As acknowledged,

graphene shows negligible stretchability. To construct stretchable electrodes, Chou et al. fabricated wrinkled graphene on PDMS by a prestraining-then-buckling strategy. Thanks to the micro-structured wrinkled structure, the graphene electrode achieved high transparency of 72.9% and a stretchability of 40%.^[29] Recently, Ha and co-workers constructed a stretchable microsupercapacitor by adopting a fractal design strategy.^[31] As shown in Figure 6g, the microsupercapacitor is generally designed into a fractal structure consisting of long and narrow patterns to ensure high transparency and stretchability. Within the microsupercapacitor, two symmetric electrodes based on MnO₂/CNT are parallelly distributed (Figure 6h). Such a fractal-designed transparent microsupercapacitor shows good mechanical stability and stable electrochemical performance upon repeated stretching cycles with 30% stretchability (Figure 6i and j). This fractal design strategy sheds light on designing other stretchable energy-storage devices.

5. Applications of Transparent Supercapacitors

To date, transparent supercapacitors have found broad applications in various types of transparent electronics including bio-sensors, laptops, transparent phones, smartwatches, smart windows, and so on (Figure 7).^[27,31,100,101] For example, Lee et al. demonstrated the application of transparent supercapacitors in a self-powered patchable sensor platform.^[100] The patchable sensor is composed of a strain sensor, a triboelectric nanogenerator, and a transparent supercapacitor, which serve as the monitor, the energy harvest and convertor, and energy storage device, respectively. To make the patchable sensor stretchable and transparent, Ag nanowire/PEDOT:PSS/polyurethane (PU) nanocomposite films were fabricated and repeatedly stacked, showing high performance, good stability, and reliability. Recently, Kim and his co-workers developed an all-transparent

wearable patch device with good electrochromic–electrochemical performances.^[27] Wearable electronics require their components to be stretchable and flexible. In this case, WO₃ nanotubes on low-density Au/Ag nanowires were embedded inside the PDMS substrate and stretchable polyacrylamide electrolytes were applied to make the whole device stretchable and flexible. The as-constructed all-transparent wearable patch device displays high transparency, good stretchability, and high reliability under repeated stretching-bending cycles. More interestingly, Park's group reported the integration of transparent supercapacitors and nanostructured metallic glass nanotroughs as skin heat patches.^[101] The full integrations consist of transparent supercapacitors, wireless antennas, heaters, and interconnects, enabling the wireless charging of supercapacitors and the heating of the heaters. Results show that such integrations are potential for thermal therapy of skin tissue, which opens a new avenue for applications of transparent supercapacitors. The applications of transparent supercapacitors are attracting ever-growing attention in recent years.

6. Summary and Outlook

Though it started just two decades ago, research on TESEs has been tremendously carried out. So far, encouraging results have been achieved and various types of TESEs emerged as promising candidates for transparent energy-storage devices, including carbon-based, polymer-based, MXenes-based, ITO-based, and metallic grids-based TESEs. Through material and structure design, high-performance TESEs with high FoM_e and FoM_c, good flexibility and stretchability can be realized. In this minireview, we introduce the evaluation metrics of TESEs to provide some basic knowledge for readers. Then, the development status of various TESEs together with their advantages and disadvantages are highlighted. More importantly, we summarize the state-of-art approaches towards high-performance TESTs, looking forward to providing some inspirations for researchers in this field.

As transparency is intrinsically conflicting with capacitance, intensive efforts are still needed to construct TESEs with desirable optical and capacitive properties. As summarized in Table 1, despite the achieved high FoM_c (up to 167 FS cm⁻²), the transparency of most TESEs is restrained below 80% due to the percolation effect. Given that many transparent applications require high transparency for their components (the touch panel requires T>85% and OLED display requires T>90%), these TESEs cannot meet the demands of transparent electronics. Improving the transparency of electrodes and devices, in turn, significantly reduces the mass loading of active materials, thus resulting in a low energy density of whole devices. From the view of energy storage, attention should also be paid to the energy densities of transparent supercapacitors, given that the mass loading of active materials of electrodes among reported works is rather low. Besides, the growth of portable and wearable electronics requires supercapacitors to be flexible, stretchable and miniaturized. At present, high FoM_c is hardly achieved in conductive substrates-free TESEs. Con-

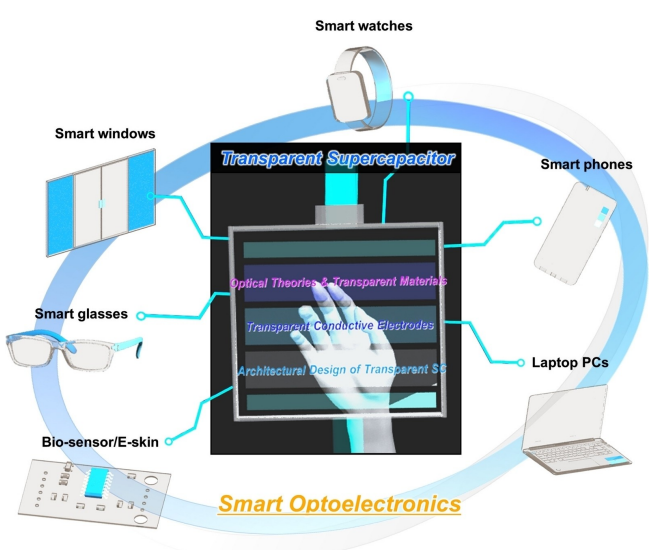


Figure 7. Applications of transparent supercapacitors in transparent electronics. Reproduced with permission from Ref. [4]. Copyright (2020) Wiley-VCH.

Table 1. Summary of optical and electrochemical performance of various types of TESEs and related supercapacitors.^[a]

Active materials	Substrates	Transparency of electrodes [%]	Areal capacitance [mF cm^{-2}]	Estimated FoM _c [FS cm^{-2}]	Transparency of devices [%]	Energy density [$\mu\text{Wh cm}^{-2}$]	Ref.
MnO ₂	Au	60	1.9	1.2	–	–	[16]
PEDOT:PSS	free	70	1.8	1.73	–	–	[17]
Ti ₃ C ₂ T _x	free	98	0.13	2.4	72	0.05	[18]
Ag–Au	Ag	88.5	0.836	2.5	–	–	[24]
MnO ₂	Au	84	2.12	4.4	82.1	0.047	[25]
SWCNT	free	–	–	–	82	0.019	[35]
SWCNT	free	90	0.584	2.04	60	–	[39]
Graphene	ITO	–	–	–	61	0.015	[43]
Graphene	free	90	0.396	1.38	71	–	[47]
Graphene	free	86	0.016	0.04	84	–	[48]
Graphene	free	72.1	19.5	20.7	50.6	0.67	[49]
Graphene	free	69.3	13.2	12.36	46.5	0.46	[50]
Graphene	free	70.2	16.84	16.4	51.6	0.58	[51]
Ni(OH) ₂ /graphene	ITO	72.3	49.25	52.7	–	–	[52]
PANI/rGO	Ag	78.76	25.6	38.06	57.4	0.57	[54]
PANI/CNT	free	55	0.55	0.3	–	–	[55]
PANI	free	82	18.5	33.4	–	–	[56]
PEDOT:PSS	free	78	4.72	6.73	58	0.38	[57]
PPy	free	72	6.56	6.93	70	0.15	[59]
PPy	Ag–Au	93	1.2	6.12	80	0.02	[61]
PEDOT	Ni	84	2.08	4.3	–	–	[62]
Ti ₃ C ₂	free	51	0.076	0.036	88	0.001	[65]
MnO ₂	ITO	55.9	11.9	6.65	44	0.42	[68]
MnO	ITO	61.6	24.6	16.9	44	0.82	[69]
Co ₃ O ₄	ITO	58	17	10.2	51	0.4	[70]
Mn ₃ O ₄	ITO	97	6.5	79.8	78	0.11	[74]
Co(OH) ₂	Ag	75	5	6.09	54	0.04	[78]
MoS ₂	Ag	70.6	23	22.8	77.5	2.453	[80]
NiCo/NiCo(OH) ₂	Ag	60.33	21.6	14.2	36.5	1.92	[83]
PEDOT	Ag	62	2.06	1.44	51	0.046	[84]
PEDOT:PSS	Ag	89	29.4	92.4	–	0.65	[86]
V ₂ O ₅ /PEDOT-G	Ag	70	22.4	21.6	55	0.18	[87]
MnO ₂	Au	86	8.26	19.88	79	0.14	[88]
MnO ₂	Au	86	3	7.21	63	0.059	[89]
PPy	Au	59.87	13.02	8.39	45	0.28	[90]
Co(OH) ₂	Ni	75	22.9	27.9	54	0.42	[93]
MnO ₂	Ni	84	80.7	167	80.82	0.94	[94]
PEDOT	Ag	84.65	3.64	7.9	77.4	0.09	[97]

[a] Note that all the FoM_c in this minireview are roughly calculated using an individual C_A and T from reported works.

ductive substrates-based TESEs, however, suffer from their rigidity nature and are challenging for use in stretchable electronics. There exists a compromise in FoM_c and stretchability. To meet the development of miniaturized electronics, fabricating TESEs through advanced technologies such as inkjet printing and screen printing will extend their applications in miniaturized products and integrated circuits.^[102–104] Pioneering works have been successively done by Zhou, Huang, and Östling's groups.^[40,47,86] We do believe that printable transparent energy-storage devices will arouse considerable interest in the future.

Previous works have demonstrated that most TESEs show undesirable transparency because of the percolation issue. Among various materials for TESTs, only PEDOT:PSS and MXenes are free from the percolation problem. Nevertheless, their energy-storage capacity is somehow low so that the achieved FoM_c is smaller compared to other types of TESEs, for example, conductive substrates-based TESEs. It is essential to improve the FoM_c of these electrodes by chemical doping or hybridization. Though MXenes consist of a large number of species, to the best of our knowledge, only Ti₃C₂T_x has been

investigated as TESEs so far. More effort should be devoted to exploring other MXenes so that more possibilities can be found.^[105] Additionally, attempts to develop new materials with excellent electrical conductivity and energy-storage capability, 2D black phosphorus and conductive metal-organic frameworks (MOFs), for example, are also encouraged.^[106,107]

Apart from TESEs, the optical and electrochemical properties of transparent supercapacitors are still unsatisfactory. As clearly shown in Figure 3, the transparency of most reported supercapacitors is located in the range between 45% and 75%, which is much lower compared to the pristine transparent TESTs. This is because conventional sandwiched assembly and the introduction of other components such as substrates and electrolytes inevitably reduce the transparency of the total device. Optimizing cell configuration by avoiding redundant components has been demonstrated to be valid for enhancing the transparency of the device. As revealed by Kulkarni et al., integrating electrodes on both sides of the separator can avoid the use of substrates, therefore improving the transparency from 64% to 78%.^[89] In addition, in-plane configuration with the presence of positive and negative electrodes on the same

plane of substrates has also been proposed for developing transparent supercapacitors with higher transparency and flexibility.^[47] Moreover, the energy density of transparent supercapacitors is still low. Sandwich-type-stacked configuration has been demonstrated advantageous to the fabrication simplicity and areal energy densities. One could obtain a higher energy density by improving the FoM_c or constructing supercapacitors in an asymmetric fashion. It still demands a vast effort in this field.

Acknowledgements

This work is supported by the National Natural Science Foundation of China (Nos. 51772116 and 51972132), and Program for HUST Academic Frontier Youth Team (2016QYTD04).

Conflict of Interest

The authors declare no conflict of interest.

Keywords: transparent electrodes • energy storage • transparent supercapacitors • evaluation metrics • strategies

- [1] R. G. Gordon, *MRS Bull.* **2011**, *25*, 52–57.
- [2] K. Ellmer, *Nat. Photonics* **2012**, *6*, 809–817.
- [3] C.-C. Kim, H.-H. Lee, K. H. Oh, J.-Y. Sun, *Science* **2016**, *353*, 682–687.
- [4] S. W. Kim, S. Y. Lee, *Energy Environ.* **2020**, doi: 10.1002/eem.212095.
- [5] H. Wu, D. Kong, Z. Ruan, P. C. Hsu, S. Wang, Z. Yu, T. J. Carney, L. Hu, S. Fan, Y. Cui, *Nat. Nanotechnol.* **2013**, *8*, 421–425.
- [6] T. Chen, L. Dai, *J. Mater. Chem. A* **2014**, *2*, 10756–10775.
- [7] Y. Xu, J. Liu, *Small* **2016**, *12*, 1400–1419.
- [8] T. Sannicolo, M. Lagrange, A. Cabos, C. Celle, J. P. Simonato, D. Bellet, *Small* **2016**, *12*, 6052–6075.
- [9] R. Wang, M. Yao, Z. Niu, *InfoMat* **2019**, *2*, 113–125.
- [10] C. Zhang, V. Nicolosi, *Energy Storage Mater.* **2019**, *16*, 102–125.
- [11] J. Chen, Y. Wang, W. Liu, Y. Ma, *ChemNanoMat* **2019**, *6*, 42–52.
- [12] P. J. King, T. M. Higgins, S. De, N. Nicoloso, J. N. Coleman, *ACS Nano* **2012**, *6*, 1732–1741.
- [13] P.-C. Chen, G. Shen, S. Sukcharoenchoke, C. Zhou, *Appl. Phys. Lett.* **2009**, *94*, 043113.
- [14] D. Wei, S. J. Wakeham, T. W. Ng, M. J. Thwaites, H. Brown, P. Beecher, *Electrochim. Commun.* **2009**, *11*, 2285–2287.
- [15] A. Yu, I. Roes, A. Davies, Z. Chen, *Appl. Phys. Lett.* **2010**, *96*, 253105.
- [16] T. Qiu, B. Luo, M. Giersig, E. M. Akinoglu, L. Hao, X. Wang, L. Shi, M. Jin, L. Zhi, *Small* **2014**, *10*, 4136–4141.
- [17] T. M. Higgins, J. N. Coleman, *ACS Appl. Mater. Interfaces* **2015**, *7*, 16495–16506.
- [18] C. J. Zhang, B. Anasori, A. Seral-Ascaso, S. H. Park, N. McEvoy, A. Shmeliov, G. S. Duesberg, J. N. Coleman, Y. Gogotsi, V. Nicolosi, *Adv. Mater.* **2017**, *29*, 1702678.
- [19] Y. Yang, S. Jeong, L. Hu, H. Wu, S. W. Lee, Y. Cui, *Proc. Natl. Acad. Sci. USA* **2011**, *108*, 13013–13018.
- [20] S. Pat, S. Ozen, V. Senay, S. Korkmaz, *Scanning* **2016**, *38*, 317–321.
- [21] A. B. Bélequé, C. Faure, M. Röder, P. Hovington, U. Posset, A. Guerfi, K. Zaghib, *Mater. Sci. Eng. B* **2016**, *214*, 81–86.
- [22] O. Kwon, H. J. Hwang, Y. Ji, O. S. Jeon, J. P. Kim, C. Lee, Y. G. Shul, *Sci. Rep.* **2019**, *9*, 3175.
- [23] S. De, T. M. Higgins, P. E. Lyons, E. M. Doherty, P. N. Nirmalraj, W. J. Blau, J. J. Boland, J. N. Coleman, *ACS Nano* **2009**, *3*, 1767–1774.
- [24] H. Lee, S. Hong, J. Lee, Y. D. Suh, J. Kwon, H. Moon, H. Kim, J. Yeo, S. H. Ko, *ACS Appl. Mater. Interfaces* **2016**, *8*, 15449–15458.
- [25] J. Yang, T. Hong, J. Deng, Y. Wang, F. Lei, J. Zhang, B. Yu, Z. Wu, X. Zhang, C. F. Guo, *Chem. Commun.* **2019**, *55*, 13737–13740.
- [26] S. Bellani, L. Najafi, G. Tullii, A. Ansaldi, R. Oropesa-Nuñez, M. Prato, M. Colombo, M. R. Antognazza, F. Bonaccorso, *J. Mater. Chem. A* **2017**, *5*, 25177–25186.
- [27] T. G. Yun, M. Park, D. H. Kim, D. Kim, J. Y. Cheong, J. G. Bae, S. M. Han, I. D. Kim, *ACS Nano* **2019**, *13*, 3141–3150.
- [28] S. Lin, X. Bai, H. Wang, H. Wang, J. Song, K. Huang, C. Wang, N. Wang, B. Li, M. Lei, H. Wu, *Adv. Mater.* **2017**, *29*, 1703238.
- [29] P. Xu, J. Kang, J.-B. Choi, J. Suhr, J. Yu, F. Li, J.-H. Byun, B.-S. Kim, T.-W. Chou, *ACS Nano* **2014**, *8*, 9437–9445.
- [30] E. P. Gilshteyn, T. Kallio, P. Kanninen, E. O. Fedorovskaya, A. S. Anisimov, A. G. Nasibulin, *RSC Adv.* **2016**, *6*, 93915–93921.
- [31] J. Yun, H. Lee, C. Song, Y. R. Jeong, J. W. Park, J. H. Lee, D. S. Kim, K. Keum, M. S. Kim, S. W. Jin, Y. H. Lee, J. W. Kim, G. Zi, J. S. Ha, *Chem. Eng. J.* **2020**, *387*, 124076.
- [32] S. De, P. J. King, M. Lotya, A. O'Neill, E. M. Doherty, Y. Hernandez, G. S. Duesberg, J. N. Coleman, *Small* **2010**, *6*, 458–464.
- [33] W. Ma, L. Song, R. Yang, T. Zhang, Y. Zhao, L. Sun, Y. Ren, D. Liu, L. Liu, J. Shen, *Nano Lett.* **2007**, *7*, 2307–2311.
- [34] A. K. Sundramoorthy, Y.-C. Wang, S. Gunasekaran, *Nano Res.* **2015**, *8*, 3430–3445.
- [35] R. Yuksel, Z. Sarıoba, A. Cirpan, P. Hiralal, H. E. Unalan, *ACS Appl. Mater. Interfaces* **2014**, *6*, 15434–15439.
- [36] L. Yu, C. Shearer, J. Shapter, *Chem. Rev.* **2016**, *116*, 13413–13453.
- [37] C. Feng, K. Liu, J.-S. Wu, L. Liu, J.-S. Cheng, Y. Zhang, Y. Sun, Q. Li, S. Fan, K. Jiang, *Adv. Funct. Mater.* **2010**, *20*, 885–891.
- [38] T. Chen, H. Peng, M. Durstock, L. Dai, *Sci. Rep.* **2014**, *4*, 3612.
- [39] Z. Niu, W. Zhou, J. Chen, G. Feng, H. Li, Y. Hu, W. Ma, H. Dong, J. Li, S. Xie, *Small* **2013**, *9*, 518–524.
- [40] P. Chen, H. Chen, J. Qiu, C. Zhou, *Nano Res.* **2010**, *3*, 594–603.
- [41] H. Lin, L. Li, J. Ren, Z. Cai, L. Qiu, Z. Yang, H. Peng, *Sci. Rep.* **2013**, *3*, 1353.
- [42] K. Lee, H. Lee, Y. Shin, Y. Yoon, D. Kim, H. Lee, *Nano Energy* **2016**, *26*, 746–754.
- [43] T. Aytug, M. S. Rager, W. Higgins, F. G. Brown, G. M. Veith, C. M. Rouleau, H. Wang, Z. D. Hood, S. M. Mahurin, R. T. Mayes, P. C. Joshi, T. Kuruganti, *ACS Appl. Mater. Interfaces* **2018**, *10*, 11008–11017.
- [44] J. J. Yoo, K. Balakrishnan, J. Huang, V. Meunier, B. G. Sumpter, A. Srivastava, M. Conway, A. L. Reddy, J. Yu, R. Vajtai, P. M. Ajayan, *Nano Lett.* **2011**, *11*, 1423–1427.
- [45] T. Chen, Y. Xue, A. K. Roy, L. Dai, *ACS Nano* **2014**, *8*, 1039–1046.
- [46] K. Jo, S. Lee, S.-M. Kim, J. B. In, S.-M. Lee, J.-H. Kim, H.-J. Lee, K.-S. Kim, *Chem. Mater.* **2015**, *27*, 3621–3627.
- [47] S. Sollami Delektta, A. D. Smith, J. Li, M. Ostling, *Nanoscale* **2017**, *9*, 6998–7005.
- [48] X. Fan, T. Chen, L. Dai, *RSC Adv.* **2014**, *4*, 36996–37002.
- [49] N. Li, X. Huang, H. Zhang, Z. Shi, Y. Li, C. Wang, *J. Mater. Chem. A* **2017**, *5*, 14595–14603.
- [50] N. Li, G. Yang, Y. Sun, H. Song, H. Cui, G. Yang, C. Wang, *Nano Lett.* **2015**, *15*, 3195–3203.
- [51] N. Li, X. Huang, H. Zhang, Y. Li, C. Wang, *ACS Appl. Mater. Interfaces* **2017**, *9*, 9763–9771.
- [52] N. Li, X. Huang, R. Li, Y. Chen, Y. Li, Z. Shi, H. Zhang, *Electrochim. Acta* **2016**, *219*, 61–69.
- [53] P. Suktha, N. Phattharasupakun, M. Sawangphruk, *Sustain. Energy Fuels* **2018**, *2*, 1799–1805.
- [54] F. Chen, P. Wan, H. Xu, X. Sun, *ACS Appl. Mater. Interfaces* **2017**, *9*, 17865–17871.
- [55] J. Ge, G. Cheng, L. Chen, *Nanoscale* **2011**, *3*, 3084–3088.
- [56] K. Devarayan, D. Lei, H.-Y. Kim, B.-S. Kim, *Chem. Eng. J.* **2015**, *273*, 603–609.
- [57] T. Cheng, Y.-Z. Zhang, J.-D. Zhang, W.-Y. Lai, W. Huang, *J. Mater. Chem. A* **2016**, *4*, 10493–10499.
- [58] M. Yoonessi, A. Borenstein, M. F. El-Kady, C. L. Turner, H. Wang, A. Z. Stieg, L. Pilon, *ACS Appl. Energy Mater.* **2019**, *2*, 4629–4639.
- [59] X. Jiao, C. Zhang, Z. Yuan, *ACS Appl. Mater. Interfaces* **2018**, *10*, 41299–41311.
- [60] H. Moon, H. Lee, J. Kwon, Y. D. Suh, D. K. Kim, I. Ha, J. Yeo, S. Hong, S. H. Ko, *Sci. Rep.* **2017**, *7*, 41981.
- [61] C. Zhang, T. M. Higgins, S.-H. Park, S. E. O'Brien, D. Long, J. N. Coleman, V. Nicolosi, *Nano Energy* **2016**, *28*, 495–505.
- [62] Y.-H. Liu, J.-L. Xu, S. Shen, X.-L. Cai, L.-S. Chen, S.-D. Wang, *J. Mater. Chem. A* **2017**, *5*, 9032–9041.
- [63] K. Hantanasirikul, M.-Q. Zhao, P. Urbankowski, J. Halim, B. Anasori, S. Kota, C. E. Ren, M. W. Barsoum, Y. Gogotsi, *Adv. Electron. Mater.* **2016**, *2*, 1600050.

- [64] J. Halim, M. R. Lukatskaya, K. M. Cook, J. Lu, C. R. Smith, L. A. Naslund, S. J. May, L. Hultman, Y. Gogotsi, P. Eklund, M. W. Barsoom, *Chem. Mater.* **2014**, *26*, 2374–2381.
- [65] P. Salles, E. Quain, N. Kurra, A. Sarycheva, Y. Gogotsi, *Small* **2018**, e1802864.
- [66] M. Mariano, O. Mashtalir, F. Q. Antonio, W. H. Ryu, B. Deng, F. Xia, Y. Gogotsi, A. D. Taylor, *Nanoscale* **2016**, *8*, 16371–16378.
- [67] B. Anasori, Y. Gogotsi, *2D Metal Carbides and Nitrides (MXenes)*, Springer, **2019**.
- [68] Y. Wang, W. Zhou, Q. Kang, J. Chen, Y. Li, X. Feng, D. Wang, Y. Ma, W. Huang, *ACS Appl. Mater. Interfaces* **2018**, *10*, 27001–27008.
- [69] J. Choi, D. Nam, D. Shin, Y. Song, C. H. Kwon, I. Cho, S. W. Lee, J. Cho, *ACS Nano* **2019**, *13*, 12719–12731.
- [70] X. Y. Liu, Y. Q. Gao, G. W. Yang, *Nanoscale* **2016**, *8*, 4227–4235.
- [71] Y. Hu, H. Zhu, J. Wang, Z. Chen, *J. Alloys Compd.* **2011**, *509*, 10234–10240.
- [72] F. Liu, X. Yang, Z. Qiao, L. Zhang, B. Cao, G. Duan, *Electrochim. Acta* **2018**, *260*, 281–289.
- [73] N. Li, C. Zhi, H. Zhang, *Electrochim. Acta* **2016**, *220*, 618–627.
- [74] I. Ryu, G. Kim, D. Park, S. Yim, *J. Power Sources* **2015**, *297*, 98–104.
- [75] X. Liu, J. Wang, G. Yang, *ACS Appl. Mater. Interfaces* **2018**, *10*, 20688–20695.
- [76] X. Liu, J. Wang, G. Yang, *Chem. Eng. J.* **2018**, *347*, 101–110.
- [77] J. L. Xu, Y. H. Liu, X. Gao, Y. Sun, S. Shen, X. Cai, L. Chen, S. D. Wang, *ACS Appl. Mater. Interfaces* **2017**, *9*, 27649–27656.
- [78] H. Sheng, X. Zhang, Y. Ma, P. Wang, J. Zhou, Q. Su, W. Lan, E. Xie, C. J. Zhang, *ACS Appl. Mater. Interfaces* **2019**, *11*, 8992–9001.
- [79] Y. Zhong, X. Zhang, Y. He, H. Peng, G. Wang, G. Xin, *Adv. Funct. Mater.* **2018**, *28*, 1801998.
- [80] J. Li, Q. Shi, Y. Shao, C. Hou, Y. Li, Q. Zhang, H. Wang, *Energy Storage Mater.* **2019**, *16*, 212–219.
- [81] H. Du, Y. Pan, X. Zhang, F. Cao, T. Wan, H. Du, R. Joshi, D. Chu, *Nanoscale* **2019**, *1*, 140–146.
- [82] S. Park, A. W. M. Tan, J. Wang, P. S. Lee, *Nanoscale Horiz.* **2017**, *2*, 199–204.
- [83] J. Liu, G. Shen, S. Zhao, X. He, C. Zhang, T. Jiang, J. Jiang, B. Chen, *J. Mater. Chem. A* **2019**, *7*, 8184–8193.
- [84] X. Liu, D. Li, X. Chen, W. Y. Lai, W. Huang, *ACS Appl. Mater. Interfaces* **2018**, *10*, 32536–32542.
- [85] G. Cai, P. Darmawan, M. Cui, J. Wang, J. Chen, S. Magdassi, P. S. Lee, *Adv. Energy Mater.* **2016**, *6*, 1501882.
- [86] T. Cheng, Y.-Z. Zhang, J.-P. Yi, L. Yang, J.-D. Zhang, W.-Y. Lai, W. Huang, *J. Mater. Chem. A* **2016**, *4*, 13754–13763.
- [87] L. Wang, T. Shu, S. Guo, Y. Lu, M. Li, J. Nzabahimana, X. Hu, *Energy Storage Mater.* **2020**, *27*, 150–158.
- [88] S. B. Singh, T. I. Singh, N. H. Kim, J. H. Lee, *J. Mater. Chem. A* **2019**, *7*, 10672–10683.
- [89] S. Kiruthika, C. Sow, G. U. Kulkarni, *Small* **2017**, *13*, 1701906.
- [90] S. Chen, B. Shi, W. He, X. Wu, X. Zhang, Y. Zhu, S. He, H. Peng, Y. Jiang, X. Gao, Z. Fan, G. Zhou, J. M. Liu, K. Kempa, J. Gao, *Adv. Funct. Mater.* **2019**, *29*, 1906618.
- [91] S. Gong, Y. Zhao, Q. Shi, Y. Wang, L. W. Yap, W. Cheng, *Electroanalysis* **2016**, *28*, 1298–1304.
- [92] Y. H. Liu, Z. Y. Jiang, J. L. Xu, *ACS Appl. Mater. Interfaces* **2019**, *11*, 24047–24056.
- [93] B. S. Soram, J. Dai, T. Kshetri, N. H. Kim, J. H. Lee, *Chem. Eng. J.* **2019**, 123540.
- [94] Y.-H. Liu, J.-L. Xu, X. Gao, Y.-L. Sun, J.-J. Lv, S. Shen, L.-S. Chen, S.-D. Wang, *Energy Environ. Sci.* **2017**, *10*, 2534–2543.
- [95] R. T. Ginting, M. M. Ovhal, J.-W. Kang, *Nano Energy* **2018**, *53*, 650–657.
- [96] J. Park, J. C. Hwang, G. G. Kim, J. U. Park, *InfoMat* **2019**, *2*, 33–56.
- [97] S. B. Singh, T. Kshetri, T. I. Singh, N. H. Kim, J. H. Lee, *Chem. Eng. J.* **2019**, *359*, 197–207.
- [98] D. L. Ma, Y. Ma, Z. W. Chen, A. M. Hu, *J. Mater. Chem. A* **2017**, *5*, 20608–20614.
- [99] J.-Y. Hong, W. Kim, D. Choi, J. Kong, H. S. Park, *ACS Nano* **2016**, *10*, 9446–9455.
- [100] B.-U. Hwang, J.-H. Lee, T. Q. Trung, E. Roh, D.-I. Kim, S.-W. Kim, N.-E. Lee, *ACS Nano* **2015**, *9*, 8801–8810.
- [101] S. Lee, S. W. Kim, M. Ghidelli, H. S. An, J. Jang, A. L. Bassi, S. Y. Lee, J. U. Park, *Nano Lett.* **2020**, *20*, 4872–4881.
- [102] C. J. Zhang, L. McKeon, M. P. Kremer, S. H. Park, O. Ronan, A. Seral-Ascaso, S. Barwich, C. O. Coileain, N. McEvoy, H. C. Nerl, B. Anasori, J. N. Coleman, Y. Gogotsi, V. Nicolosi, *Nat. Commun.* **2019**, *10*, 1795.
- [103] L. Wang, S. Chen, T. Shu, X. Hu, *ChemSusChem* **2020**, *13*, 1330–1353.
- [104] S. Abdolhosseinzadeh, R. Schneider, A. Verma, J. Heier, F. Nuesch, C. J. Zhang, *Adv. Mater.* **2020**, e2000716.
- [105] J. Yi, J. Li, S. Huang, L. Hu, L. Miao, C. Zhao, S. Wen, V. N. Mochalin, A. M. Rao, *InfoMat* **2019**, *2*, 601–609.
- [106] P. Nakhanivej, X. Yu, S. K. Park, S. Kim, J. Y. Hong, H. J. Kim, W. Lee, J. Y. Hwang, J. E. Yang, C. Wolverton, J. Kong, M. Chhowalla, H. S. Park, *Nat. Mater.* **2019**, *18*, 156–162.
- [107] D. Sheberla, J. C. Bachman, J. S. Elias, C. J. Sun, Y. Shao-Horn, M. Dinca, *Nat. Mater.* **2017**, *16*, 220–224.

Manuscript received: August 6, 2020

Revised manuscript received: August 22, 2020

Accepted manuscript online: August 24, 2020

Version of record online: September 10, 2020